Comparison of Wind and Wave Fields between High-Resolution Simulations and Operational Forecast Products: A Case of Wave Development under Easterly Wind Jets in the West of the Tsugaru Strait

Teruhisa SHIMADA and Hiroshi KAWAMURA

Ocean Environment Group, Center for Atmospheric and Oceanic Studies,
Graduate School of Science, Tohoku University
Aramaki Aza Aoba 6-3, Aoba-ku, Sendai, Miyagi PREF 980-8578 Japan

Corresponding author: Teruhisa Shimada
e-mail: shimada@ocean.caos.tohoku.ac.jp
Tel: +81-22-795-6747, Fax: +81-22-795-6748

Keywords: MM5, SWAN, GPV, wind wave, Yamase

Received 28 July 2008; accepted 29 September 2008

Abstract

We compare high-resolution simulated wave fields with operational wave forecasts under easterly coastal wind jets in the west of the Tsugaru Strait from a case study on 5-9 June 2003. We use a series of numerical simulations by one-way coupling between a mesoscale meteorological model and a shallow-water wave model with high spatiotemporal resolutions of 2 km and 1 hour. The simulated wind fields represent pairs of small-scale wind jets blowing from the coast and their confluence to form a large wind jet. These features are consistent with those revealed by a high-resolution wind field derived from RADARSAT. The wave simulations reflect the features of the wind fields and show localized higher wave regions under the wind jets. At the same time, the simulations show peaks of significant wave height corresponding to each small-scale wind jet. The wave energy spreading from the higher wave region reaches the surrounding coast. On the other hand, the operational forecast products of wind and wave with 10-km resolution reproduce the only main wind jet blowing through the strait and a corresponding high wave region. Wave energy spreading toward the coast and time evolutions of wave development are not represented. This study shows the limitation of the operational forecasts and proposes a required resolution for accurate forecasts of coastal wind and wave.

1. Introduction

Wave simulations with higher spatiotemporal resolution are indispensable for better forecast and hindcast of coastal waves. High spatial resolution simulations can improve the geometry of the coastline and topographical features and reflect detailed features of wind fields (Cavaleri and Bertotti, 2004). Simulations with high temporal resolutions allow us to investigate evolution of wave. Due to the technical improvements and sophisticated algorithm developments, it has been verified that recent wave models have applicability to high-resolution simulations of coastal waves (e.g., Gorman and Neilson, 1999; Wornon et al., 2001; Rogers et al., 2003; Signell et al., 2005; Shimada and Kawamura, 2006; Isoguchi and Kawamura 2007; and Shimada et al. 2008). However, it is still a crucial challenge to obtain wind input whose resolution is comparable to the wave model performance and is high enough to capture the coastal wind variations. In fact, the above-mentioned studies have shown the limit of application of general operational wave products to coastal wave forecasts and hindcasts. Global/regional weather products provided by operational service still generally do not have a spatiotemporal resolution of the models required to accurately forecast coastal wind and wave. At the same time, evaluation of the operational wave forecasts to discuss the limit of their application has not been available yet near the Japanese coast.

Wave development under gap exiting winds is one

of the cases in which high-resolution capability is strongly required for both wind and wave simulations. Thus, we focus on the wave development under the gap exiting winds. We choose an area in the west of the Tsugaru Strait during the warm half-year as a case study (Fig. 1). In June-August, the wind often blows from the Pacific Ocean toward the Tohoku District and Hokkaido, associated with the high-pressure system over the Sea of Okhotsk. This northeasterly/easterly wind usually persists for several days and accompanies cool and wet air, low-level clouds and fogs due to a thin mixed layer and an upper stable layer (e.g., Ninomiya and Mizuno, 1985). The wind is known as Yamase (e.g., Takai et al., 2006). These characteristics of Yamase promote the formation of locally intensified winds (i.e. wind jets) in the terrestrial gaps. Shimada and Kawamura (2007) have mentioned several pairs of strong and weak wind regions in the west of the Tsugaru Strait along the coast of the Japan Sea. However, it is the only study on localized strong winds in this area and detailed distributions of wind and wave have not been described.

This study investigates wind and wave distributions under the easterly wind jets in the west of the Tsugaru Strait from a case study on 5-9 June 2003 and compares wind and wave fields represented by high-resolution simulations and operational mesoscale forecast products. We make use of one-way coupling of a mesoscale meteorological model and a shallow-water wave model with 2-km and 1-hour resolutions in space and time. The case is selected because the easterly winds are persistent during the case study period. Specific questions we would like to address are: 1) What are the structural properties of the strong winds and high waves in the west of the Tsugaru Strait? 2) How much does the resolution difference have an impact of the wind and wave distributions?

This study has the following significances. First, the present study can specify the limit of application of the operational wave product, which is used for public coastal wave forecast. In fact, we point out possible localized high wind and wave for practical use. Enhanced services relevant to sea conditions are required for various field activities over the ocean such as ocean shipping, marine security, and marine disaster prevention. Then, understanding of localized winds leads to the study of coastal ecosystems because wind variations are significantly important for ocean circulation especially in the coastal seas. It

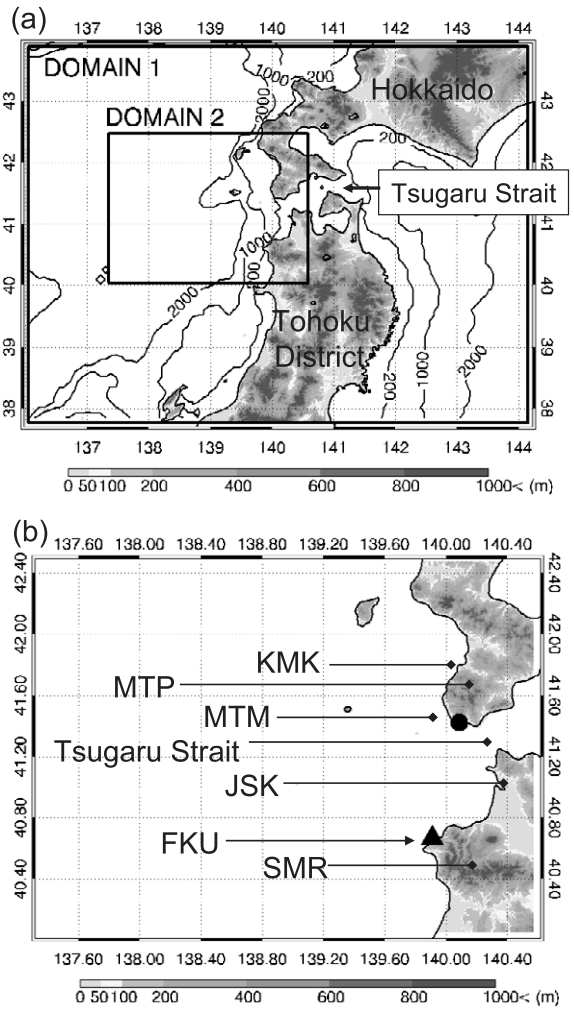

Fig. 1. (a) Map of the topography and geographical locations referred to in this paper. The two MM5 model domains are indicated by the rectangles. The color scale overland, in these figures and others to follow, indicates the terrain elevation. The contours are isobaths of 200, 1000, and 2000 m. The inner domain (Domain 2) of MM5 is also the domain of the SWAN simulation. (b) A closeup of Domain 2. The solid circle indicates an AMeDAS station. The triangle indicates a NOWPHAS wave observation station. Abbreviations are geographical and station names: KMK Kaminokuni; MTP: Matsumae Peninsula; MTM Matsumae; JSK Jyusanko; FKU Fukaura; and SMR Shirakami mountain range.

is verified by satellite observations that the localized strong wind can activate oceanic ecosystems due to the resulting upwelling and mixing (e.g., Hu and Liu, 2003; Samuelsen and O'Brien, 2008). Finally, this study deals with the final stage of the air-sea-land interaction induced by Yamase. A great number of stud-

ies have been made on Yamase because agriculture in the Tohoku District is subject to cool summer damage induced by Yamase and because accompanying cloud and fog influence aviation and marine navigation. However, little attention has been given to the wind after passing through the strait and the resulting wave field.

We give brief data descriptions and model simulation frameworks in the following section. In section 3, we illustrate simulated wind and wave fields to compare with observations and operational products. Section 4 is devoted to summary and concluding remarks.

2. Data and Model

We use two types of Grid Point Value (GPV) data provided by the Japan Meteorological Agency (JMA). One is the 6-hourly objectively analyzed data at a 10-km grid interval produced by Meso-scale Non-hydrostatic Model (MSM) in order to give initial and boundary conditions for meteorological simulations. The other is GPV wave forecast data at a 10-km grid interval in order to compare with the simulated wave field. The GPV wave forecast data are produced by JMA using the GPV MSM wind data, and contain analyzed fields every 12 hours (0000 and 1200 UTC) and forecasts every 6 hours (0600 and 1800 UTC). For meteorological simulation, the daily merged SST maps (Guan and Kawamura, 2004) are averaged to make a constant ocean surface boundary condition. We use the following four datasets to verify the model simulation results. 1) Ocean surface wind vectors observed by SeaWinds/QuikSCAT at 12.5-km resolution. 2) The RADARSAT-derived wind field with a resampled grid interval of 500 m using a scatterometer model function and the polarization ratio conversion factor (Thomson and Beal, 2000) with wind direction from the GPV MSM data. 3) Hourly wind observations at a station overland acquired by automatic observation facilities, called AMeDAS (Automated Meteorological Data Acquisition System) operated by JMA (Fig.1b). 4) Significant wave height (SWH) data recorded every two hours by a wave observation station called NOWPHAS (Fig.1b).

Model simulation efforts in this study are made with the Pennsylvania State University-NCAR (PSU-NCAR) fifth-generation Mesoscale Model MM5 [Grell et al., 1995] and a third generation wave model SWAN (Simulating WAves Nearshore) [Booij et al. 1999; Ris et al. 1999]. Hourly surface wind fields simulated by MM5 are used to drive the SWAN simulation. For MM5 simulation, we define two model domains with grid size of 6- and 2-km as shown in Fig.1a. The inner domain of MM5 is the same with the SWAN model domain. They have a grid spacing of 2 km and an hourly temporal resolution in common. Because this case study satisfies the fetch-limited condition and we focus on only wind-generated waves, incoming waves at the open boundaries of the model domain are assumed to be zero. The SWAN model is run in non-stationary mode. According to the method of Shimada and Kawamura (2008), the result in stationary mode at 0900 UTC 6 June 2003 is used as an initial condition. The MM5 simulation is initialized at 0000 UTC 5 June 2003 and integrated to 0000 UTC 10 June 2003 during 120 hours. The SWAN simulation is initialized at 0900 UTC 6 June 2003 and integrated to 0000 UTC 10 June 2003 during 87 hours. The detail model setups and one-way coupling methodology follow Shimada and Kawamura [2008].

3. Results and Discussion

3.1. Observations of wind jets in the west of the Tsugaru Strait

Between 5 and 9 June 2003, the easterly wind blows persistently toward the Tohoku District and Hokkaido. The MM5 simulation begins on 5 June, when a high-pressure system over the Sea of Okhotsk started to develop and a low-pressure system moved eastward on the southern coast of Japan according to the weather charts (not shown). Then, the center of the high-pressure system moved southward from the Sea of Okhotsk to the southeast side off Hokkaido, accompanying the easterly wind. With the southward movement of the high-pressure system, the easterly wind gradually shifted to the south over the study area (Fig.1a). The end of the MM5 simulation corresponds to this timing. The persistent easterly wind is one of the characteristics of Yamase. The series of wind fields from SeaWinds measurements and their descriptions during the study period are given in Shimada and Kawamura [2007].

We first show that wind jet is captured in wind speed time series of a meteorological station data (Fig. 2), and pinpoint the timing of the focus of this study. Because an AMeDAS station MTM is located at the western exit of the Tsugaru Strait, it is an appropri-

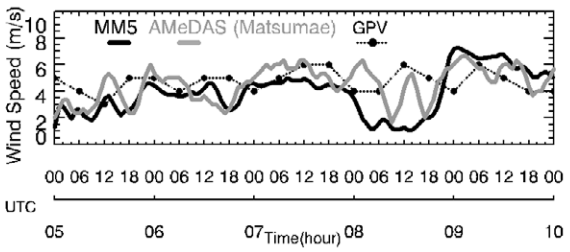

Fig. 2. Hourly time series of wind speeds at station Matsumae (gray) and derived from MM5 (black) at the corresponding grid during 5-9 June 2003. Wind speeds from six hourly GPV data are also plotted (dotted black line with black circles).

ately positioned meteorological station to capture the wind jet event among available stations. While wind speeds are 3-6 m/s before 1800 UTC 8 June, wind speed increases rapidly after that time. The satellite wind observations in Fig. 3 are obtained during the intensification of the wind jet. Hereafter we focus on the wind and wave fields at 1800 UTC 8 June. This is because the wind distributions do not change so much after the onset of the wind jet at 1800 UTC 8 June, and because GPV data available at 1800 UTC 8 June is closest to the observations. The simulated wind speeds by MM5 are also shown in Fig. 2. While the simulated time series underestimate the wind variations during 0000-1800 UTC 8 June, the wind speeds and their variations are generally consistent with the observations. The average difference between the simulated and observed wind speed is -0.61 m/s and the correlation coefficient is 0.62. This supports the validity of the MM5 simulations. Six-hourly wind speeds from the GPV data are also plotted at the corresponding grid. The GPV wind speeds apparently seem to be close to the observations and simulations because of the fluctuations between 4 and 6 m/s. However, it is difficult to say that the GPV wind can well represent the wind variations during the term.

Fig. 3 shows wind fields observed by SeaWinds/QuikSCAT at 12.5-km resolution and derived from RADARSAT at a resampled resolution of 500 m. In the 12.5-km wind field (Fig.3a), we can identify a major wind jet blowing from the western exit of the Tsugaru Strait and a part of a minor wind jet at 42.0 °N/139.2°E. The SeaWinds observations within 20 km of coastlines are not available because of possible land contamination. On the other hand, the wind field

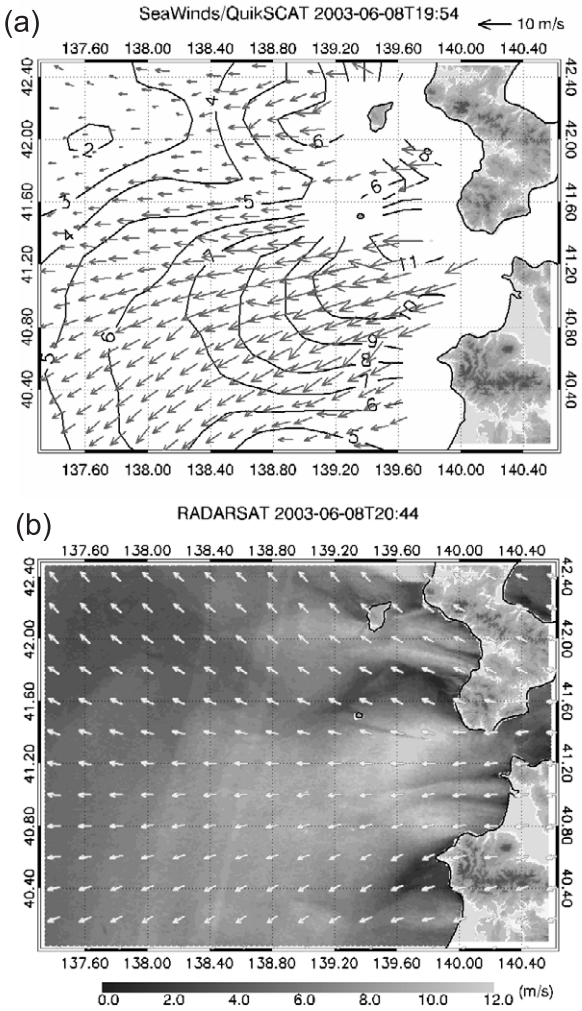

Fig. 3. (a) Ocean surface wind vectors measured by SeaWinds/QuikSCAT at 1954 UTC June 8 2003. The contours indicate wind speed. (b) Wind field derived from RADARSAT at 2044 UTC June 8 2003. The arrows of equal length indicate wind direction extracted from the GPV MSM data.

derived from RADARSAT reveals the detailed structure of winds near the coast. We can see several pairs of strong and adjacent weak wind regions along the coast. It is clearly confirmed that the two wind jets inferred from the SeaWinds observations are composed of a few of small-scale wind jets with several-kilometer width. It is possible to trace weak wind regions between the strong wind jets over the 50-km at least from the coast. The wind maxima are located just after passing through the coastal tips at 41.4° N/139.8°E and 40.8°N/139.8°E. Wind is blocked by the mountainous areas (MTP and SMR) and weak winds are observed in the lee. The wind speeds are much smaller than inferred from the SeaWinds ob-

servations. Comparison of these wind fields makes us to recognize anew that high-resolution capability is indispensable for accurately illustrating wind fields near the coastline. Thus, this RADARSAT-derived wind field serves to evaluate the performance of the wind simulations.

3.2. High-resolution simulated fields of wind and wave

Fig. 4 shows wind and wave fields simulated by MM5 and SWAN at 1800 UTC 8 June 2003. The simulated wind field (Fig. 4a) with a grid interval of 2 km well reproduces the detail structures revealed by the RADARSAT-derived wind field (Fig. 3b). The time difference between them is not important here. This is because the simulated wind distributions change little over the sea surface for the next six hours though the overland wind speed increases rapidly at station MTM (Fig.2) after 1800 UTC 8 June 2003. It is confirmed in Fig. 4a that the small-scale wind jets blowing from the coast merge to form one large wind jet with keeping the weaker wind region between them. While the wind speeds in the lee of the mountainous area (MTP and SMR) are a little smaller than the observations in Fig.3b, the shapes of the distributions of weak winds are quite similar.

The simulated SWH field by SWAN at 1800 UTC 8 June 2003 is shown in Fig.4b. The SWH field reflects the features of the wind field in Fig.4a. We first should note the two peaks of SWH greater than 0.85 m at 40.9°N/139.6°E and 41.2°N/139.6°E. They result from wind jets blowing from the west exit of the Tsugaru Strait and a small terrestrial gap upwind of JSK. While the lower SWH region is can be traced along the weak wind region between the wind jets, the two peaks of SWH merge to form a large high SWH region. The high SWH region extends toward the southwest along the wind direction. Higher waves from the main high wave region reaches the coast near SMR due to wave directional spreading. In the lee of MTP, lower SWH region extends downwind toward the northwest. On the north of it, higher SWH region extend toward the northwest, being partly blocked by the island. We can confirm two peaks of SWH greater than 0.40 m at 41.9°N/139.7°E and 42.0° N/139.7°E, whose locations correspond to the wind jets.

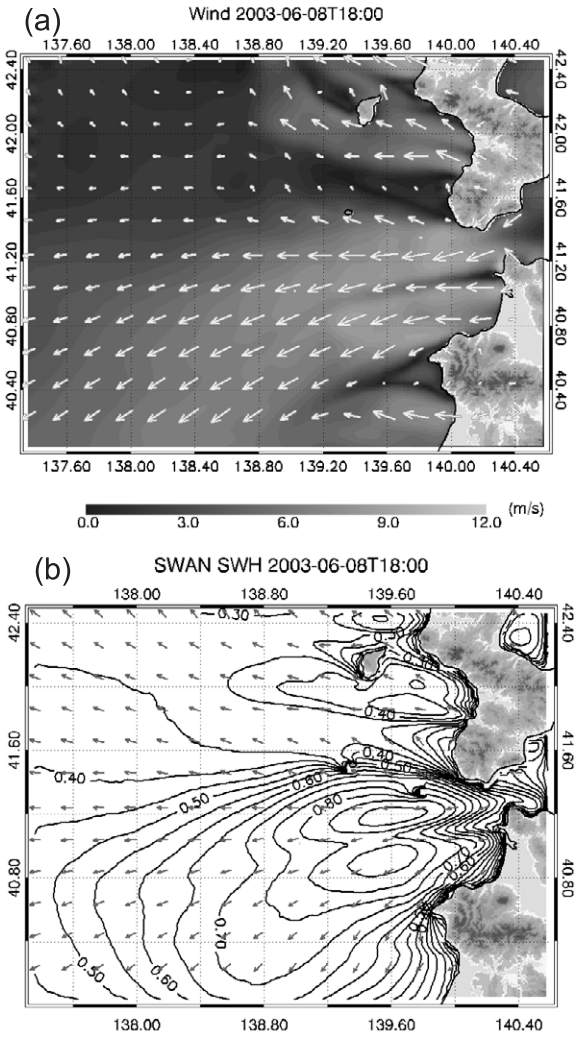

Fig. 4. (a) Simulated wind field by MM5 at 1800 UTC June 8 2003. Grayscale shade indicates wind speed. (b) Simulated significant wave height field by SWAN at 1800 UTC June 8 2003. The arrows of equal length indicate mean wave direction.

3.3. Operational wave forecast field

Fig. 5 shows wind and wave fields from the GPV data at 1800 UTC 8 June 2003. These 10-km fields are the finest-resolution products operated by JMA for daily weather forecast. In the wind field (Fig. 5a), only one wind jet is reproduced in the west of the Tsugaru Strait. While the maximum wind speed is close to that of the observation, the structures of the wind jets are totally different. The location of the wind maximum shifts westward. The wind jets extending from JSK and KMK are not reproduced, and there are no indications of the lower wind regions in the lee of MTP and SMR.

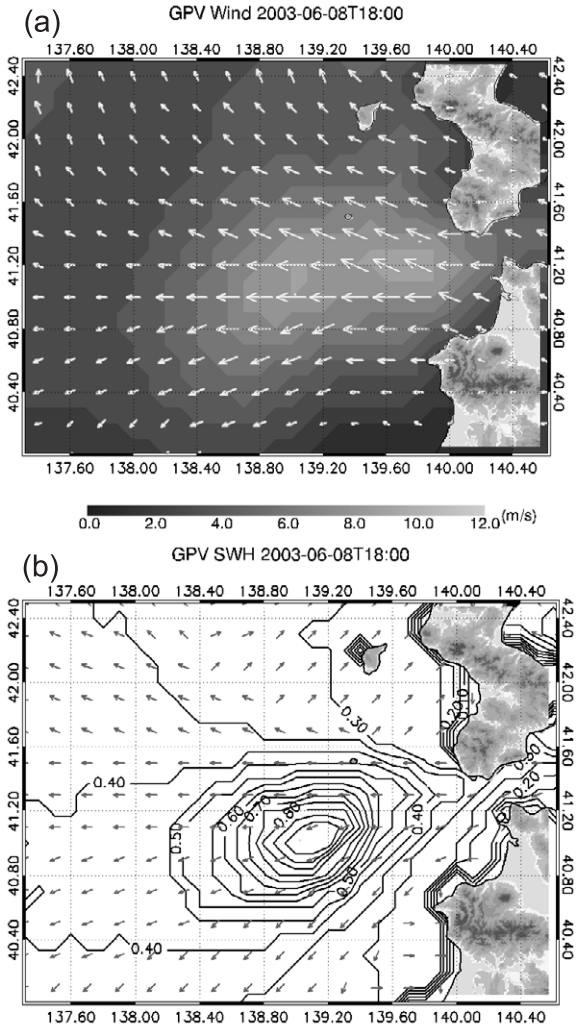

Fig. 5. (a) Wind vector field by GPV MSM at 1800 UTC June 8 2003. Grayscale shade indicates wind speed. (b) Significant wave height field by GPV data at 1800 UTC June 8 2003. The arrows indicate mean wave direction.

Such wind distribution is reflected in the wave field (Fig.5b). While the highest SWH is almost the same with that of the SWAN simulation, the higher wave region is located westward at 41.0°N/139.2°E. Contrary to the SWAN simulation, the two peaks of SWH are not reproduced. The high wave region is localized concentrically and its broadening is too small to reach the coast near station FKU. Consequently, wave development within 30 km of the coastlines is underestimated.

Finally we show in Fig. 6 SWH time series of the observation, the SWAN simulation, and the GPV data. SWH is sampled at a grid corresponding to wave station FKU. While the station is not located downwind on the main axis of the wind jets from

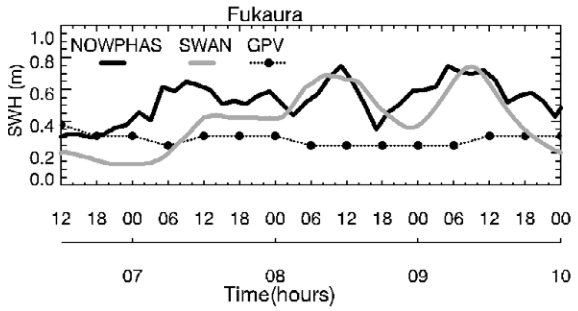

Fig. 6. Two-hourly significant wave height recorded at stations FKU (solid black line) from 1200 UTC June 6 2003 to 0000 UTC June 10 2003. Hourly simulated significant wave heights by SWAN (solid gray line) and GPV data (dotted black line with black circles) at the corresponding point are also shown.

the Tsugaru Strait, the station is expected to observe the waves spreading from the high wave region. The observed SWH generally ranges from 0.5 to 0.7 m during 7-9 June, and shows two peaks at 1100 UTC 8 June and at around 0900 UTC 9 June. While the SWAN simulation underestimates the SWH by 0.1-0.2 m before 0000 UTC 8 June, the simulation result is generally consistent with the observations. Particularly, the simulation is capable of predicting the two SWH peaks. On the other hand, the SWH from the GPV data is almost constant at 0.3 m during the study period. This means that waves near the shore are hardly predicted. In fact, the spreading effect of high waves is not taken into account because the wind jets are not reproduced well (Fig. 5a).

4. Summary and Concluding Remarks

We have compared high-resolution wave simulations and operational wave forecasts under coastal wind jets in the west of the Tsugaru Strait from a case study on 5-9 June 2003. The simulated fields of wind and wave with 2-km and 1-hour spatiotemporal resolutions are compared with operational wave forecasts with 10-km and 6-hourly spatiotemporal resolutions. The following conclusions are obtained.

1) The high-resolution wind field derived from RADARSAT with a 500-m grid interval reveals wind jets blowing from terrestrial gaps. The major wind jet blowing from the Tsugaru Strait merges with small wind jets to form a large wind jet. Merging of wind jets is also observed along the coast of Hokkaido. Wind blocking is seen in the lee of the mountainous areas. Maximum

wind speed differences are up to 8 m/s between the neighboring strong and weak wind regions. These features are well reproduced by the MM5 simulations.

2) The simulated wave fields by SWAN with a grid interval of 2-km well reflect the features of the wind fields. The simulated SWH field represents SWH peaks corresponding to each wind jet and wave blocking in the lee of the islands. The variation of SWH is consistent with observations.

3)Wind forecasts with a 10-km grid interval from the GPV data represent only one localized strong winds in the west of the Tsugaru Strait. While the maximum wind speeds are close to the observations, the distributional shapes of the strong winds are different from those of high-resolution observations and simulations. No other small wind jets can be reproduced. While 10-km wave forecasts represent the localized high wave region, the forecasts do not show two SWH peaks corresponding to the wind jets and wave blocking due to the islands. The GPV wave forecasts have difficulty replicating coastal SWH variation due to the spatiotemporal resolution.

Looking back the results above, we can draw the following conclusions. First, consideration of high-resolution wind fields is an important starting point for accurate wave forecasts. Though we have taken this fact for granted, unpredictable distributions of coastal wind can be revealed by high-resolution observations in some cases. Wave development under a gap exiting wind is one of the cases in which high-resolution capability is strongly required for both wind and wave simulations. For example, alternating strong and weak wind region affect the directional properties of waves [Shimada and Kawamura, 2006]. Then, we have proposed a resolution required to describe winds and wind waves in this study area. Terrestrial gaps with width of 5-15 km can form a wind jet extending over 100 km. A small island can block the wave and leave a long tail of lower wave height. These topographic features must be resolved adequately in the simulations. Finally we should note that monitoring of the wind jet development and high waves is only possible at limited locations. Examination of high-resolution observations and simulations can provide us with a chance to reconsider and improve the configuration and network of observation systems. Understanding of strong winds and severe waves in coastal seas are important not only for studying intense air-sea interaction but also for practical use such as shipping, marine security, and marine disaster prevention. The transmission of such information is becoming more important for the appropriate agencies or communities. Regional forecast is also expected to satisfy the above demands.

Acknowledgements

The authors would like to thank the members of Physical Oceanography Group of Tohoku University for their valuable advice on a regular basis. AMeDAS and GPV MSM data were provided by the Japan Meteorological Agency. We purchased JMA GPV wave forecast data from the Japan Weather Association. We obtained NOWPHAS data from the Marine Environment and Engineering Department of the Port and Airport Research Institute. J-EGG500 (Japan Oceanographic Data Center-Expert Grid data for Geographic-500m) bathymetric data were used for the wave simulation. Use of MM5 is made possible by the National Center of for Atmospheric Research. The authors thank SWAN team for making SWAN available. The MM5 and SWAN simulations are carried out using the supercomputer system of Cyberscience Center, Tohoku University. This study is supported by Exploratory Research Program for Young Scientists of Tohoku University.

References

Booij, N., R. C. Ris and L. H. Holthuijsen (1999) A third-generation wave model for coastal regions, Part I, Model description and validation. J. Geophys. Res., C4, 104: 7649-7666.

Cavaleri, L. and L.Bertotti, (2004) Accuracy of the modelled wind and wave fields in enclosed seas. Tellus, 56A: 167-175.

Gorman, R. M. and C. G.Neilson (1999) Modelling shallow water wave generation and transformation in an intertidal estuary. Coastal Eng., 36: 197-217.

Grell, G., J. Dudhia and D. Stauffer (1995) A Description of the Fifth-Generation Penn State/ NCAR Mesoscale Model, (MM5). NCAR Tech. Note, 398, 122 pp.

Guan, L. and H. Kawamura (2004) Merging satellite infrared and microwave SSTs: Methodology and evaluation of the new SST. J. Oceanogr., 60: 905-912.

Hu, H. and W. T. Liu (2003) Oceanic thermal and biological responses to Santa Ana winds. Geophys. Res. Lett., 30 (11): 1596, doi:10.1029/2003GL017208/

Isoguchi, O. and H. Kawamura (2007) Coastal wind jets flowing into the Tsushima strait and their effect on wind waves. J. Atmos. Sci., 64: 564-578.

Ninomiya, K. and H. Mizuno (1985) Anomalously cold spell in summer over Northeastern Japan caused by northeasterly wind from polar maritime air-mass. Part 2. Structure of the northeasterly flow from polar maritime airmass. J. Met. Soc. Japan, 63: 859–871.

Ris, R. C., N. Booij and L. H. Holthuijsen (1999) A third-generation wave model for coastal regions, Part II, Verification. J. Geophys. Res. C4, 104: 7667-7681.

Rogers, W. E., P. A. Hwang, and D. W. Wang (2003) Investigation of wave growth and decay in the SWAN Model: Three regional-scale applications. J. Phys. Oceanogr., 33: 366-389.

Samuelsen, A. and J. J. O'Brien (2008) Wind-induced cross-shelf of water masses and organic matter at the Gulf of Tehuantepec. Deep-Sea Res. I, 55: 221-246.

Signell, R. P., S. Carniel, L. Cavaleri, J. Chiggiato, J. D. Doyle, J. Pullen and M. Sclavo (2005) Assessment of wind quality for oceanographic modelling in semi-enclosed basins. J. Mar. Sys., 53 (1-4): 217-233.

Shimada, T., and H. Kawamura (2006) Wind-wave development under alternating wind jets and wakes induced by orographic effects. Geophys. Res. Lett., 33, L02602, doi:10.1029/2005GL025241.

Shimada, T., and H. Kawamura (2007) Case study of wind jet transition and localized responses of wind wave along the Pacific coast of northern Japan by synergetic use of satellite and in situ observations. J. Oceanogr., 63: 953-966.

Shimada, T. and H. Kawamura (2008) Numerical simulations of wind wave growth under coastal wind jet through the Kanmon Strait, Wea. Forecasting, 23(6): 1162-1175.

Takai, H., H. Kawamura and O. Isoguchi (2006) Characteristics of the Yamase Winds over oceans around Japan observed by the scatterometer-derived ocean surface vector winds. J. Met. Soc. Japan, 84(2): 365-373.

Thomson, D. R.and R. C. Beal (2000) Mapping high-resolution wind fields using synthetic aperture radar, Johns Hopkins Univ. Tech. Dig., vol.21: 58-67.

Wornom, S. F., D. J. S. Welsh and K. W. Bedford (2001) On coupling the SWAN and WAM wave models for accurate nearshore wave prediction. Coastal Eng. J., 43 (3): 161-201.